CONDENSED MATTER PHYSICS

Proof of the elusive high-temperature incommensurate phase in CuO by spherical neutron polarimetry

Navid Qureshi[1]*, Eric Ressouche[2], Alexander Mukhin[3], Marin Gospodinov[4], Vassil Skumryev[5,6]

CuO is the only known binary multiferroic compound, and due to its high transition temperature into the multiferroic state, it has been extensively studied. In comparison to other prototype multiferroics, the nature and even the existence of the high-temperature incommensurate paraelectric phase (AF3) were strongly debated—both experimentally and theoretically—since it is stable for only a few tenths of a kelvin just below the Néel temperature. Until now, there is no proof by neutron diffraction techniques owing to its very small ordered Cu magnetic moment. Here, we demonstrate the potential of spherical neutron polarimetry, first, in detecting magnetic structure changes, which are not or weakly manifest in the peak intensity and, second, in deducing the spin arrangement of the so far hypothetic AF3 phase. Our findings suggest two coexisting spin density waves emerging from an accidental degeneracy of the respective states implying a delicate energy balance in the spin Hamiltonian.

INTRODUCTION

Multiferroic materials combine at least two of the ferroic orders [(anti)ferromagnetism, ferroelectricity, ferroelasticity, and ferrotoroidicity] and have been extensively studied in the last two decades [see (1, 2) and references therein]. Of particular interest are magnetoelectric multiferroics that have (anti)ferromagnetic and ferroelectric order since such a system reveals new opportunities of storing data in future memory and multifunctional devices. In so-called type II or improper multiferroics, the onset of a complex magnetic order goes along with breaking of inversion symmetry, and the resulting ferroelectric polarization due to atomic shifts is induced by the magnetic order. In such a case, the electric properties could be manipulated via a magnetic field and vice versa. In a type I or proper multiferroic material, the two orders have different origins, take place at different temperatures, and are therefore very weakly or not coupled. Complex inversion-symmetry breaking magnetic structures in improper multiferroics are often a result of geometrical frustration, and therefore many materials revealing these properties have very low transition temperatures into the multiferroic state. Understanding the properties of high-temperature multiferroics—for the search or tailoring of new materials pushing the limits even further—has been at the center of recent multidisciplinary research.

The appearance of a macroscopic electric polarization induced by an inversion-symmetry breaking magnetic structure at 230 K makes CuO (tenorite) the bulk material with the second-highest transition into the multiferroic state (3) after $YBaCuFeO_5$ (4–6). The spin arrangement (7–10) in the so-called AF2 phase was already investigated 30 years ago, and it was notably the spherical neutron polarimetry (SNP) work by Brown et al. (9) that allowed an unambiguous determination of the associated magnetic structure: an incommensurate oblique helix with spins rotating in a plane with slight inclination with regard to the plane perpendicular to the propagation

vector **q**. This spin rotation plane or spin envelope is defined by two main axes b and α, where the latter lies within the a-c plane, at 28° from the positive c toward the positive a axis (11). The electric polarization along the monoclinic axis b (space group $C2/c$) may result from the cycloidal component via the inverse Dzyaloshinskii-Moriya effect (11–14), although the actual mechanism remains under debate (15–19) and several other alternative mechanisms, e.g., involving magnetic frustration and magnetostriction, have been proposed. The direct relation between the chiral spin helix and the electric polarization was demonstrated in an SNP experiment by switching the chiral domains with an applied electric field (20). Below 213 K down to low temperatures, CuO reveals a commensurate collinear antiferromagnetic structure (AF1) that conserves inversion symmetry and is therefore paraelectric. The high transition temperatures reflect the strong Cu-Cu exchange, which was investigated by both ab initio methods and inelastic neutron scattering [see (21) and references therein].

The usual magnetic phase transition sequence of type II multiferroics (Fig. 1), e.g., $Ni_3V_2O_8$ (22, 23) and $MnWO_4$ (24, 25), upon cooling, is first a high-temperature incommensurate phase (AF3) with longitudinal amplitude modulation followed by a low-temperature incommensurate phase (AF2) of complex noncentrosymmetric cycloidal nature inducing a ferroelectric polarization. The ground state (AF1) is a commensurate antiferromagnet with the same moment direction as in the AF3 phase. The variety of magnetic phases is a consequence of the temperature-dependent competition between single-ion anisotropy and exchange interactions (26).

The existence of the AF3 phase in CuO was first promoted in (27) based on the praphase concept. Within this approach, it was shown that the AF2 phase is characterized by two one-dimensional irreducible representations, while both AF1 and AF3 are characterized by only one. Furthermore, it was argued that the Cu spins point along the b axis in the AF3 phase. The necessity for an incommensurate collinear AF3 phase was also justified by the analysis of the nonlocal Landau-type free energy based on a mean-field treatment of a Heisenberg-type Hamiltonian (15). The same moment direction was predicted, but only half of the Cu spins are believed to order. On the other hand, Monte Carlo studies based on first-principles calculations failed to reproduce its existence (16, 17). A phenomenological theory of phase transitions in CuO was suggested in (18),

[1]Institut Laue-Langevin, 71 Avenue des Martyrs, 38042 Grenoble Cedex 9, France. [2]Université Grenoble Alpes, CEA, IRIG, MEM, MDN, F-38000 Grenoble, France. [3]Prokhorov General Physics Institute, Russian Academy of Sciences, ul. Vavilova 38, Moscow 119 991, Russia. [4]Institute of Solid State Physics, Bulgarian Academy of Sciences, 1784 Sofia, Bulgaria. [5]Departament de Física, Universitat Autònoma de Barcelona, 08193 Bellaterra, Barcelona, Spain. [6]Institució Catalana de Recerca i Estudis Avançats, 08010 Barcelona, Spain.
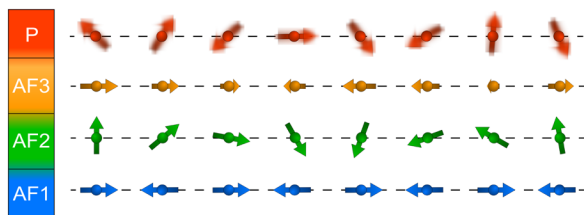*Corresponding author. Email: qureshi@ill.fr

Fig. 1. Usual magnetic phase transition sequence in type II multiferroics. In the paramagnetic state (P), the magnetic moments are fluctuating (represented by blur) and condense into the high-temperature incommensurate phase AF3 at T_N, which consists of an amplitude modulation with spins pointing along the magnetic easy axis. In the low-temperature incommensurate phase AF2, the spins adopt a cycloidal modulation before they align in a commensurate antiferromagnetic structure (AF1) at low temperature.

in which a direct first-order phase transition PM→AF2 was described. CuO was argued to exhibit an inverted sequence of symmetry-breaking mechanisms with respect to other type II multiferroics. Ultrasound velocity (11, 15) and thermal expansion (28) measurements indeed suggest a third magnetically ordered phase just below the Néel temperature with a temperature stability range of less than 0.5 K. Being close to the elevated Néel temperature, the ordered magnetic moment μ is very small, and therefore no neutron diffraction study was able to clarify the existence and the nature of this phase. However, to understand the complete picture of CuO and—especially by comparing it to related compounds—type II multiferroics in general, the microscopic structure of this AF3 phase is of major importance since the sequence of magnetic phase transitions and their associated magnetic structures are a result of the competition between exchange interactions and single-ion anisotropy that govern the physics of the system. This provides information to potentially develop a Hamiltonian able to better explain the mechanism of multiferroicity in CuO.

The study presented here uses the SNP technique yielding two key advantages, which presumably makes it the unique microscopic probe to prove and study the AF3 phase: (i) It is extremely sensitive to the direction of the ordered magnetic moments, and (ii) conclusive results can be obtained on just a few magnetic Bragg peaks. The observed intensity in conventional unpolarized neutron diffraction is proportional to the square of the magnetic interaction vector $\mathbf{M}_\perp$, and very subtle changes in the spin alignment, especially if they happen continuously over a very narrow temperature range, can easily be missed. Furthermore, a unique magnetic structure model can only be proposed by refining it to tens or hundreds of reflections. In the case of the AF3 phase in CuO, it is impossible to measure such a large number of magnetic reflections with reasonable counting statistics owing to the very small ordered Cu moment. In polarized neutron scattering, the spin of the incident neutron is rotated by 180° around $\mathbf{M}_\perp$ for purely magnetic scattering [and for the case that the real and imaginary parts of $\mathbf{M}_\perp$ are parallel, for perpendicular real and imaginary parts, the incident neutron polarization is rotated toward the cross product of Re($\mathbf{M}_\perp$) and Im($\mathbf{M}_\perp$), i.e., toward **Q**] independently of the size of the magnetic moment. SNP not only offers direct access to the two components of $\mathbf{M}_\perp$ but also allows the full three-dimensional reconstruction of the neutron spin rotation after the interaction with the sample, which is routinely measured and summarized in the so-called polarization matrix. This yields incomparable precision concerning the direction of the mag-

netic moments in the investigated sample and is decisive for this study (see Materials and Methods for more information).

RESULTS

SNP experiments were carried out using the same sample as in our previous work (11). To access magnetic reflections modulated with the incommensurate propagation vector $\mathbf{q} = (q_h\ 0\ q_l)$, the sample was mounted with its b axis vertical (with a precision of approximately 2°) in a two-axis setup. For purely magnetic Bragg reflections as they are observed in CuO, the polarization matrix **P** with matrix elements $P_{f,i}$ takes the following form

$$\mathbf{P}_{f,i} = \begin{pmatrix} \dfrac{-p_0 M^2 - J_{yz}}{I_x} & \dfrac{-J_{yz}}{I_y} & \dfrac{-J_{yz}}{I_z} \\[2ex] 0 & \dfrac{p_0\left(M_{\perp y}^2 - M_{\perp z}^2\right)}{I_y} & \dfrac{p_0 R_{yz}}{I_z} \\[2ex] 0 & \dfrac{p_0 R_{yz}}{I_y} & \dfrac{p_0\left(-M_{\perp y}^2 + M_{\perp z}^2\right)}{I_z} \end{pmatrix} \quad (1)$$

where $M^2 = \mathbf{M}_\perp \mathbf{M}_\perp^*$, $M_{\perp y}^2 = M_{\perp y} M_{\perp y}^*$, and $M_{\perp z}^2 = M_{\perp z} M_{\perp z}^*$. The off-diagonal terms are $R_{yz} = 2\mathrm{Re}(M_{\perp y} M_{\perp z}^*)$ and $J_{yz} = 2\mathrm{Im}(M_{\perp y} M_{\perp z}^*)$, where the latter results from chiral scattering. The respective matrix elements are normalized to the scattered intensity depending on the initial neutron polarization ($I_x = M^2 + p_0 J_{yz}$, $I_y = I_z = M^2$); p_0 is the polarization of the incoming beam. The reference frame usually used in polarized neutron scattering defines the x direction to be parallel to **Q**, z to be vertical, and y to complete a right-handed coordinate system. A more detailed description of the SNP technique can be found in Materials and Methods and in (29).

For ($h0l$) ± **q** reflections in the aforementioned sample geometry the z axis is parallel to b and the y axis is in the a-c plane. From Eq. 1, it is easy to deduce that the polarization matrix of the (0.5 0 –0.5) reflection within the collinear AF1 phase (μ||b) has zero off-diagonal elements and $P_{xx} = P_{yy} = -P_{zz} = -1$, if one assumes perfect neutron polarization. Figure 2 shows the temperature dependence of the rocking curves (Fig. 2A), integrated intensities (Fig. 2B), and the polarization matrix elements P_{yy} and P_{xy} (Fig. 2C). It can be seen that for the AF1 phase, below 213 K, the P_{yy} term proves to be in accordance with the collinear antiferromagnetic structure with μ||b. At 213 K, a first-order phase transition takes place into the AF2 phase evidenced by the abrupt change of P_{yy} to a value of ~−0.1 and also from the jump in the integrated intensity. At approximately 227 K, the P_{yy} term starts to rise and saturates at a plateau of approximately $P_{yy} = 0.2$ at 228.8 K before it drops to zero at 229.3 K. The increase in P_{yy} with increasing temperature is a clear and unambiguous indication for a larger α component, whereas due to the weak scattered intensity, it is not possible to observe a change in the integrated intensities. The temperature stability range of this modified magnetic structure can be estimated from the points of steepest increase and decrease of P_{yy} and results in roughly 0.5 K. Both the change in P_{yy} and the stability range are clear proofs for the existence of the AF3 phase in CuO.

The correct description of magnetic domains (see sections S1 and S2) is crucial for the analysis of polarimetry data. In principle, without any external force, the population of the magnetic domains can be assumed to be close to equal. However, we observe nonzero chiral terms P_{xy} and P_{xz} within the AF2 phase, implying an imbalance
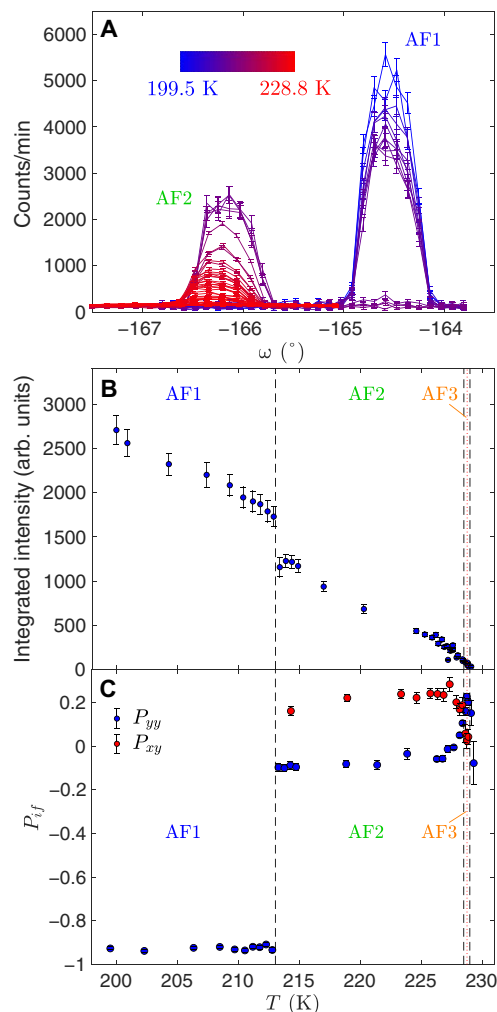
Fig. 2. Temperature dependence of the neutron intensity and polarization measured on the magnetic (000) + q peak. (**A**) The rocking scans over the incommensurate ($\omega \approx -166.2°$) and commensurate ($\omega \approx -164.6°$) peak positions at different temperatures (from 199.5 K shown in blue to 228.8 K shown in red with a linear color gradient in between) revealing the change of the propagation vector. The corresponding integrated intensities are depicted in (**B**). In (**C**), the P_{yy} term indicates the first-order transition from the AF1 to the AF2 phase at 213 K, which is also visible as a jump in the integrated intensities. At 228 K, a moderate increase toward a maximum value of 0.22 indicates the transition into the AF3 phase before the polarization drops to 0 above T_N (a close-up of this region is shown in Fig. 5A). Note that the ordered moment is too small to see a change in the intensities. The black dashed lines mark the phase boundaries, and the red dotted line denotes the temperature at which the data collection within the AF3 phase was carried out.

of chiral domain populations. This favorable situation allowed us to follow the chiral term P_{xy} as a function of temperature. An optical second harmonic generation study revealed that the domain distribution is stable throughout the entire AF2 temperature range (*30*). Consequently, the chiral term is directly proportional to the projection of the spin envelope along the scattering vector, allowing us to probe a rotation or a squeeze of this spin envelope. As it can be seen in Fig. 2C, the chiral P_{xy} term of the (000) + **q** reflection becomes negligible just when entering the AF3 phase, which can be explained by two types of magnetic structures: (i) a purely cycloidal modula-

tion, since **Q** = **q**, and by definition of a cycloid, one of the Fourier components is parallel to **Q** and does not contribute to magnetic scattering, which yields $J_{yz} = 0$, or (ii) a sinusoidally modulated magnetic structure.

In the first part of the experiment, we have measured full polarization matrices in the AF1 and AF2 phases, which yield excellent agreement ($\chi^2 = 2.8$ for AF1 and $\chi^2 = 1.6$ for AF2) with the known magnetic structures (see more details in section S3). The observed and calculated elements of the polarization matrices are shown in Fig. 3 (A and B).

It can be easily shown (see section S4) that the observed P_{yy} and P_{zz} terms within the AF3 phase cannot be explained by a single irreducible representation. Therefore, spin-density wave (SDW) phases with the ordered moment along the *b* or the α direction can be excluded as well as a nonchiral spin helix as similarly proposed for MnWO$_4$ (*25*). With the information deduced from the temperature dependence of the P_{xy} term, we can rule out a helical modulation of the AF3 phase, since this would not explain the disappearance of the chiral term at the AF2→AF3 phase transition. A purely cycloidal modulation, as mentioned above, would in principle agree with zero chiral terms; however, there is no structure model, which would satisfy all observed polarization matrix elements measured at $T = 228.8$ K. We therefore concentrated on sinusoidally modulated magnetic structures and found a solution where the magnetic structure is a collinear SDW of the same symmetry as the AF2 phase with the ordered moment direction between the two easy directions of the system, i.e., between the *b* and the α axis (see refinement results in Fig. 3C). The refined Fourier components of the Cu spin in the AF3 phase are $\mathbf{S}_{AF3} = [0.21(2)\ 0.27\ 0.30(1)]\ \mu_B$, while the population of the two orientational domains has been refined to 49(5)% and 51(5)% ($\chi^2 = 3.6$). From the temperature dependence of the integrated intensity and the calculated structure factors for the AF1 and AF3 models, we can estimate the ordered magnetic moment amplitude to be approximately 0.06 μ_B. The resulting magnetic structure, in comparison to AF2, is shown in Fig. 4 will be discussed in the following section.

DISCUSSION

In comparison with other type II multiferroics revealing a subsequent condensation of order parameters—one applying to the longitudinal and one to the transversal moment component with respect to **q**—the case in CuO is a bit different, since the AF2 structure is closer to a helix than to a cycloid. Nevertheless, if one continues in the analogy, each of the main axes of the spin envelope in the AF2 phase should be modulated by a different irreducible representation Γ, while only one representation is necessary to describe the AF1 phase. This works well for the AF1←→AF2 phase transition, with the *b* component being modulated according to Γ_1 and the α component being modulated according to Γ_2. However, it is not possible to explain the observed data in the AF3 phase with a single irreducible representation requiring the assumption of a mixed representation.

CuO is an interesting system in terms of magnetic anisotropy. Clearly, the easy axis is defined by the collinear AF1 ground state with the moments pointing along the *b* axis (see Fig. 4D). However, within the AF2 phase, the system reveals an easy-plane character, since the spins rotate within a circular envelope containing the *b* axis and the α direction. This second direction is also apparent when a large enough magnetic field is applied along the *b* axis at low temperatures (*11*), which results in a spin-flop transition aligning the
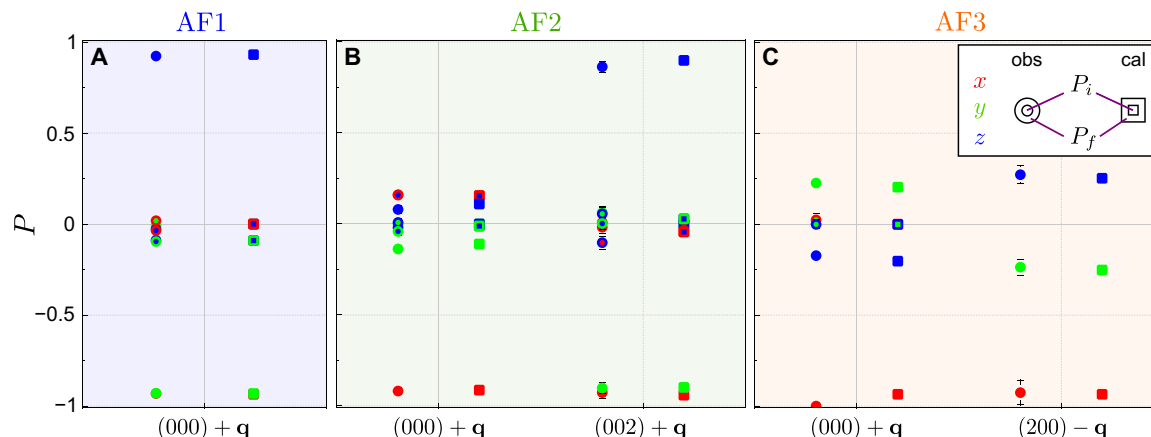
Fig. 3. Results of the refinement to the SNP data. (**A**) The commensurate AF1 phase at 200 K, (**B**) the helical AF2 phase at 215 K, and (**C**) the so far uncharacterized AF3 at 228.8 K. Circles represent the observed polarization values, while squares show the refinement for the different magnetic Bragg reflections labeled on the horizontal axis. The color code identifying the different $P_{f,i}$ elements is given as an inset in (C), e.g., a blue symbol with red edge means P_{xz}. All observed (obs) and calculated (cal) values are listed in table S1.

spins close to α (see Fig. 4C). Now, the results concerning the AF3 phase suggest a collinear arrangement in between those two special directions at approximately 51° from the *b* axis toward the α direction.

A single-phase scenario with mixed representations $\Gamma_1 + \Gamma_2$ can arise due to a competition of various contributions to the magnetic anisotropy—including terms of eighth order with respect to the order parameters along the *b* and the α directions, which would reveal a coincidence of their temperature instability, i.e., an accidental degeneracy leading to a higher-order multicritical point. In the usual interpretation of Landau theory, the combination of two representations is only allowed for the successive condensation of two order parameters. However, we note that the AF3-AF2 phase transition might be accomplished via a change of the phase shift $\Delta\varphi$ between components of the order parameters belonging to Γ_1 and Γ_2, i.e., from $\Delta\varphi = 0$ (π) in AF3 to $\Delta\varphi = \pi/2$ ($-\pi/2$) in AF2, which could occur by means of either a first-order transition or two second-order ones through intermediate values, corresponding to low-symmetry magnetic modes (four chiral and rotational domains)—as we will further test. In the former case, the first-order transition could expand to some finite temperature range due to a phase coexistence.

A second interpretation of our data is possible, which again involves both the *b* and the α direction to be energetically equivalent, which is motivated by the circular spin-rotation envelope within the AF2 phase. The AF3 phase can be described as a coexistence of two SDW phases, one with μ||*b* (Fig. 4D) and the other with μ||α (Fig. 4C). Two SDW phases, corresponding to each of the irreducible representations, may appear at the same temperature as a result of a first-order phase transition between them, which implies their coexistence in a certain temperature range. This phase coexistence takes place due to a certain combination of parameters of magnetic interactions and their temperature dependences in CuO, which results in a unique thermodynamic path along the line of the first-order transition between two SDW sinusoidal phases. This scenario is congruent with the experiment (see section S5). The phase volume of the first configuration would result in $P_{yy} = -0.935$, whereas the second configuration yields $P_{yy} = 0.935$. However, due to the different magnetic interaction vectors of the two configurations, the resulting observed polarization would not average to 0 for all magnetic Bragg reflections, even for a homogeneous distribution of the two separated phases.

Within each of the coexisting SDW phases according to Γ_1 or Γ_2, respectively, the population of the configurational domains does not affect the respective polarization matrices (see section S2). Therefore, the phase volumes ϕ can be refined by weighting the theoretical polarization values $P_{f,i}$ and scattered intensities I of the phases described by Γ_1 and Γ_2 for both observed reflections [calculated with Mag2Pol (*31*) based on the magnetic structure models assuming equally sized spins] according to

$$P_{f,i} = \frac{\phi^{\Gamma_1} P_{f,i}^{\Gamma_1} I^{\Gamma_1} + \phi^{\Gamma_2} P_{f,i}^{\Gamma_2} I^{\Gamma_2}}{\phi^{\Gamma_1} I^{\Gamma_1} + \phi^{\Gamma_2} I^{\Gamma_2}} \qquad (2)$$

For our sample at $T = 228.8$ K, this yields $\phi^{\Gamma_1} = 35(1)\%$ and $\phi^{\Gamma_2} = 65(1)\%$ ($\chi^2 = 2.8$). The calculated [observed] values are $P_{yy} = 0.21$ [0.23(2)] and $P_{zz} = -0.21$ [−0.17(2)] for the (000) + **q** reflection and $P_{yy} = -0.27$ [−0.24(4)] and $P_{zz} = 0.27$ [0.27(5)] for the (200) − **q** reflection.

A similar phase separation of different irreducible representations was theoretically predicted in the $Er_2Ti_2O_7$ pyrochlore compound in which the long-range order—resulting from the order-by-disorder phenomenon—is driven from the ψ_2 to the ψ_3 state upon Y doping as a consequence of the competition of structural disorder with thermal and quantum fluctuations (*32, 33*). A frozen mosaic of ψ_2 and ψ_3 domains was indeed observed experimentally (*34*).

In the two-phase scenario, the transition into the multiferroic AF2 phase would presumably take place by a continuous increase of the respective perpendicular component within each phase forming an elliptical spin envelope, which becomes circular at approximately 227.5 K evidenced by the saturating chiral polarization term and the corresponding value of P_{yy}. In the one-phase scenario, the transition can be interpreted as a simultaneous increase and rotation of the spin envelope—close to the AF3 phase being defined by a large axis along the [0.21(2) 0.27 0.30(1)] direction with a small axis perpendicular to it within the *b*α plane ($\Delta\varphi \approx 0$)—toward the main anisotropy axes of the helical structure ($\Delta\varphi = \pi/2$), for which two possibilities exist: either the SDW moment direction rotates toward the *b* axis or toward the α direction. Note that a deviation of the order parameter from being parallel or perpendicular to the monoclinic axis results in the presence of four magnetic domains during the second-order phase transition (see section S2). The simulation results are
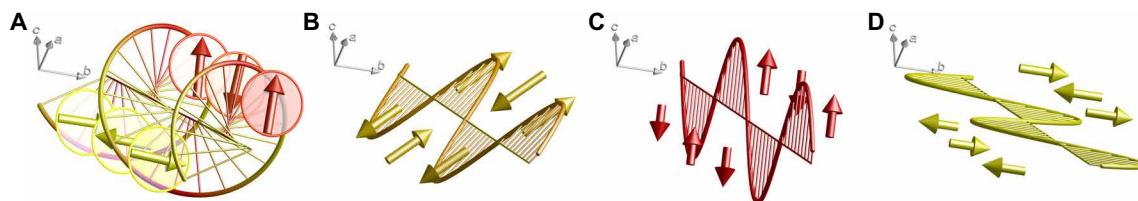
Fig. 4. Magnetic structure models. (**A**) Helical magnetic structure in the AF2 phase focusing on a part of a Cu-zigzag chain and showing a right-handed rotation (emphasized by the spiral) of the magnetic moments along the propagation vector. The circular envelope is depicted around the spins, where the b direction is represented in yellow and the α direction is in red. (**B** to **D**) Collinear sinusoidally modulated magnetic structures with magnetic moments along a direction in between b and α modulated by $\Gamma_1 + \Gamma_2$ (B), along the α direction modulated by Γ_2 (C), and along the b axis modulated by Γ_1 (D). The amplitude modulation is emphasized by sine waves.

shown in Fig. 5A, and the different scenarios are shown schematically in Fig. 5B. The transition of the spins was assumed to be linear in temperature, and at each temperature, the expected spin configuration was used together with the previously derived domain populations (one-phase scenario) or phase volumes (two-phase scenario) to calculate the polarization matrix and extract the P_{yy} and P_{xy} elements (note that a nonlinear temperature variation of the spins would in fact only shift and/or compress/expand the calculated curve on the temperature axis). The resulting values are shown together with the same data points as in Fig. 2B focusing on the AF2→AF3 transition. It can be seen that the two-phase scenario captures the temperature dependence of the polarization values very well, while the one-phase scenarios reveal a substantially different tendency for the P_{yy} terms. Note that a superposition of the two one-phase scenario curves would coincide with the two-phase scenario curve; however, this would imply the necessity of including an additional magnetic domain for which there is no justification from symmetry considerations: (i) Those two domains cannot be related by any symmetry operator due to the special direction of the spin component in the AF3 phase, and (ii) the maximum number of possible domains is four due to the group-subgroup relation of the nuclear and magnetic symmetry.

Last, we will discuss the possibility of a temperature-dependent population of chiral domains in the transition from the AF2 to the AF3 phase. In that case, the thermodynamic imbalance of chiral domains in the AF2 phase would gradually be leveled due to thermal fluctuations when approaching AF3. The polarization data in the AF3 phase at 228.8 K can then be equally well explained with an elliptic helix, $\mathbf{S}_{AF3} = [i*0.15\ 0.195(4)\ i*0.22]$, yielding a 28% compression of the spin envelope along b. Alternatively, a coexistence of the AF2 circular helix [53(3)%] with a $\mu \| \alpha$ SDW is equivalent. These models suggest a transition from a circular helix ($\Gamma_1 + \Gamma_2$) to a phase described by Γ_2, which, however, cannot be reconciled with the temperature dependence of the P_{yy} term. On approaching a pure Γ_2 state, one would expect a steadily increasing value in the temperature range 228.8 K $< T < T_N$, but it can be seen in Fig. 5A that P_{yy} reaches a plateau of approximately 0.2, which is defined by the two data points just below 229 K revealing similar error bars at the same counting time, before it drops to 0. The existence of a pure Γ_2 state would imply a significantly larger value of P_{yy} at $T = 228.87$ K, which is still inside the AF3 phase as compared to the data point at 229.1 K with a considerably larger error bar due to the vanishing ordered magnetic moment.

CONCLUSIONS

Using SNP, we have derived unambiguous proof for the existence of the elusive AF3 phase in CuO, which, to date, could not be observed
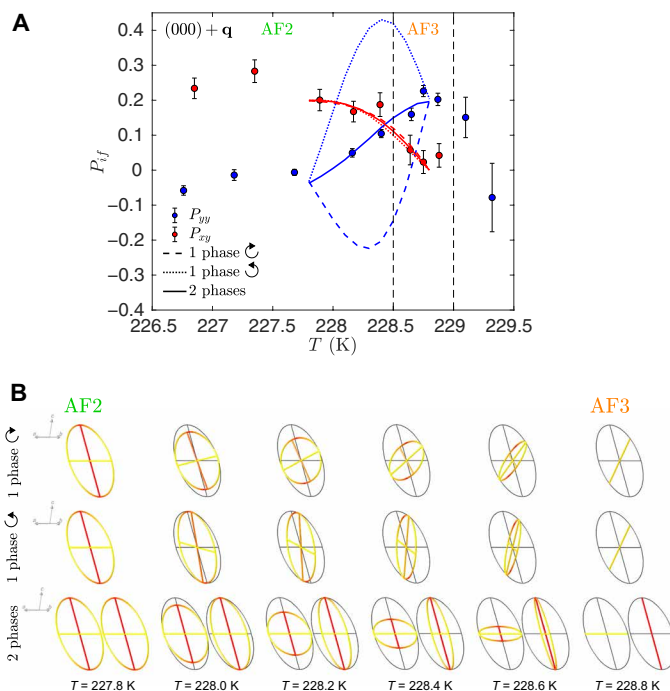

Fig. 5. Simulated phase transition between the AF2 and AF3 phases. (**A**) The data points are the same as in Fig. 2B. Dashed and dotted lines represent the one-phase scenario for the two different possibilities: The SDW moment direction moves toward the b axis, or the SDW moment direction moves toward the α direction, respectively, with a simultaneous increase of the perpendicular component. Solid lines show the expected polarization values for a coexistence of two SDW structures in the AF3 phase with a gradual increase of the respective perpendicular component for decreasing temperature. (**B**) Perspective view on the spin envelopes at six different temperatures (shown in red and yellow for components along α and b, respectively) in comparison to the circular envelope deep within the AF2 phase (shown in gray). Rows 1 and 2 depict the simultaneous rotation and expansion (for the two cases mentioned above) of this envelope when going from the AF3 to the AF2 phase in the one-phase scenario. In the last row, the two-phase scenario is sketched, showing two envelopes at each temperature representing the two coexisting SDW phases. In each of those phases, the component perpendicular to the SDW moment direction increases upon cooling until the circular spin envelope is reached in both phases at $T = 227.8$ K.

using neutron scattering methods. Our data suggest that the associated magnetic structure is incompatible with an SDW phase corresponding to a single-order parameter being modulated by a single irreducible representation. Instead, we have revealed that the AF3 phase has two spin components, which lie along the α and b directions belonging to two different irreducible representations. The

magnetic structure is best described as a coexistence of two SDW phases with the ordered moment direction along either of the main axes of the AF2 phase modulated by one irreducible representation.

Our results reveal unique microscopic information concerning the AF3 phase and the magnetic anisotropy in CuO with the α direction appearing energetically slightly more favorable just below the Néel temperature. The latter could be considered as a bicritical or tetracritical point of the corresponding phase diagrams in the parameter space of critical thermodynamic coefficients. This adds an extremely important missing piece to the puzzle of the complex behavior of magnetic phases in this extensively studied multiferroic compound. The full description of the magnetic symmetry and the accidental degeneracy of order parameters supply valuable ingredients for further theoretical studies, which will help to better understand this system with outstanding position in the family of magnetically induced ferroelectrics and multiferroics in general.

MATERIALS AND METHODS
Spherical neutron polarimetry
In addition to the general law in magnetic neutron scattering that only the component of the magnetic structure factor perpendicular to the scattering vector $\mathbf{Q}$ (generally denoted as the magnetic interaction vector $\mathbf{M}_\perp$) contributes to magnetic scattering, neutrons with their polarization axis parallel to $\mathbf{M}_\perp$ will undergo a non–spin-flip scattering process, while neutrons with polarization perpendicular to $\mathbf{M}_\perp$ will be scattered with a spin-flip. Magnetic structures like helices or cycloids reveal chiral scattering, which is polarization dependent and will create or annihilate polarization along the scattering vector $\mathbf{Q}$ and can therefore be revealed by analyzing the final neutron polarization along the $\mathbf{x}$ direction (in polarized neutron experiments, a local reference frame is defined for every Bragg reflection, where $\mathbf{Q}\|\mathbf{x}$, $\mathbf{z}$ is vertical and $\mathbf{y}$ completes the right-handed set). The direct access to the two components of $\mathbf{M}_\perp$ is the key advantage of SNP compared to conventional unpolarized neutron scattering, which is visualized in Fig. 6. Furthermore, it is possible to fully reconstruct the three-dimensional rotation of the neutron spin after the interaction with the sample including the created or annihilated polarization. The final neutron spin $\mathbf{P}_f$ is related to the initial one by

$$\mathbf{P}_f = \mathcal{P}\mathbf{P}_i + \mathbf{P}' \tag{3}$$

where $\mathcal{P}$ is a rotation matrix acting on the initial neutron spin $\mathbf{P}_i$ and $\mathbf{P}'$ is the created/annihilated polarization. By aligning the initial neutron polarization along the directions x, y, or z and by analyzing the component of the final neutron spin along these directions, one can summarize nine measurements in the so-called polarization matrix, which is better defined as a pseudomatrix, since it combines the rotation and the created/annihilated polarization. For the general case, i.e., including nuclear, magnetic, and interference terms as well as different degrees of polarization and analyzer efficiency for the different directions, the polarization matrix is

$$\mathbf{P}_{f,i} = \begin{pmatrix} \dfrac{p_{ix}(N^2 - M^2) - J_{yz}}{p_{fx}} & \dfrac{-p_{iy}J_{nz} - J_{yz}}{p_{fx}} & \dfrac{p_{iz}J_{ny} - J_{yz}}{p_{fx}} \\[2mm] \dfrac{p_{ix}J_{nz} + R_{ny}}{p_{fy}} & \dfrac{p_{iy}(N^2 + M_{\perp y}^2 - M_{\perp z}^2) + R_{ny}}{p_{fy}} & \dfrac{p_{iz}R_{yz} + R_{ny}}{p_{fy}} \\[2mm] \dfrac{-p_{ix}J_{ny} + R_{nz}}{p_{fz}} & \dfrac{p_{iy}R_{yz} + R_{nz}}{p_{fz}} & \dfrac{p_{iz}(N^2 - M_{\perp y}^2 + M_{\perp z}^2) + R_{nz}}{p_{fz}} \end{pmatrix} \tag{4}$$
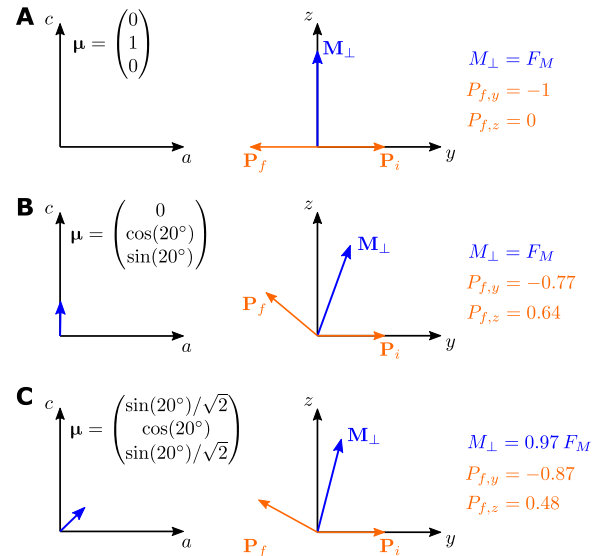
Fig. 6. Comparison between SNP and conventional unpolarized neutron scattering. A simple Néel order with $\mathbf{q} = (0.5\ 0\ 0)$ on a primitive single-domain cubic lattice with one magnetic atom in the unit cell is assumed. The magnetic moment of fixed size (shown as blue arrows projected onto the a-c plane on the left-hand side sketches) is chosen (**A**) along the b axis, (**B**) 20° inclined from b toward c, and (**C**) 20° inclined from b toward the $\langle 101 \rangle$ direction. The sketches on the right-hand side show the corresponding local reference frames for a $\mathbf{Q} = (000) + \mathbf{q}$ reflection together with the magnetic interaction vector $\mathbf{M}_\perp$, the incident neutron polarization $\mathbf{P}_i$ ($\mathbf{P}_i\|y$ in this illustration) and the final neutron polarization $\mathbf{P}_f$. For each magnetic moment configuration, the modulus of the expected $\mathbf{M}_\perp$ (compared to the magnetic structure factor F_M) and the two components of $\mathbf{P}_f$ are given. Note that unpolarized neutrons do not reveal any difference between cases (A) and (B) and that a 3% change of $M_\perp$ in (C) can also be accounted for by a 3% smaller ordered moment. SNP clearly differentiates between the three cases—with a precision of approximately 1 to 2% of the respective components $P_{f,y}$ and $P_{f,z}$—independently of the ordered moment size.

The additional terms in comparison to Eq. 1 are $N^2 = NN^*$ (N is the nuclear structure factor), $R_{ny} = 2\text{Re}(NM_{\perp y}^*)$, $R_{nz} = 2\text{Re}(NM_{\perp z}^*)$, $J_{ny} = 2\text{Im}(NM_{\perp y}^*)$, and $J_{nz} = 2\text{Im}(NM_{\perp z}^*)$, while $I_x = N^2 + M_{\perp y}^2 + M_{\perp z}^2 + p_{ix}J_{yz}$, $I_y = N^2 + M_{\perp y}^2 + M_{\perp z}^2 + p_{iy}R_{ny}$, and $I_z = N^2 + M_{\perp y}^2 + M_{\perp z}^2 + p_{iz}R_{nz}$. In the absence of nuclear scattering, i.e., for purely magnetic peaks, $N = R_{ny} = R_{nz} = J_{ny} = J_{nz} = 0$. By further assuming the same degree of incident neutron polarization ($p_{ix} = p_{iy} = p_{iz} = p_0$) and analyzer efficiency for the three directions as well as correcting the data for the latter ($p_{fx} = p_{fy} = p_{fz} = 1$), one obtains the polarization matrix shown in Eq. 1.

The polarized neutron diffraction experiment was carried out at the hot neutron polarized diffractometer D3 (ILL, Grenoble) using a wavelength of $\lambda = 0.85$ Å. A standard orange cryostat was placed within the cryogenic polarization device in a two-axis geometry. Note that an applied electric field along the b axis would have produced a majority chiral domain. However, since it is not known how an electric field affects the stability of the AF3 phase, and since it might stabilize the AF2 phase, we have decided to study the sample in its thermodynamic equilibrium. The sample was mounted with its b axis along the vertical axis of the diffractometer. The orientation was achieved using neutron Laue diffraction (OrientExpress, ILL) with a precision of approximately 2°. Guide fields in the order of a few tens of milligauss were used to maintain the neutron polarization along the beam path and to rotate it within directions perpendicular

to the direction of flight. The precession coils—decoupled from the outer guide fields and the zero-field sample chamber by an inner and outer superconducting Meissner shield—allow the three-dimensional manipulation of the neutron spin. The neutron spin analysis was carried out using polarized ^{3}He spin-filter cells whose time-dependent efficiency was monitored with calibration measurements by periodically monitoring the P_{zz} term of a nuclear reflection, which, for perfect neutron polarization and spin-filter efficiency, should always be 1. The actual observed value is a product of the expected value, the initial neutron polarization ($p_0 = 0.935$ on the D3 diffractometer), and the spin-filter efficiency [$p_{He}(t)$ between 0.85 and 0.95 for this experiment]. The time-dependent decay of the monitored values revealed a half-time of approximately 100 hours for the used cells, which were replaced every 24 hours by a new one revealing a flipping ratio of approximately 16. All data shown have been corrected for this time-dependent decrease of the spin-filter efficiency, but not for the incident polarization, since if chiral scattering is present, not all polarization matrix elements depend on the neutron polarization in the same way (see Eq. 1 or 4).

The measuring procedure for every single element of the polarization matrix consists in counting the spin-up (n^+) and spin-down neutrons (n^-) in the detector by flipping the analyzed polarization typically every second, which yields $P_{f,i} = (n^+ - n^-)/(n^+ + n^-)$. The polarization values have been corrected by measuring the background on both sides of the Bragg peak.

The search for a phase with a very narrow temperature stability range requires considerable instrumental effort. Therefore, before starting any measurement, the temperature was stabilized for 30 min even for temperature changes of 0.1 K, and we could assure a temperature stability throughout the measurements of a few hundredths of a kelvin.

To determine the magnetic structures in the different phases, full or partial polarization matrices were recorded on different magnetic Bragg reflections. The analysis of the polarimetry data was performed using the software Mag2Pol (*31*), which is able to refine magnetic structure models with symmetrical constraints and multiple magnetic domains.

Single-crystal neutron diffraction
The temperature dependence of selected magnetic reflections was measured on the single-crystal neutron diffractometers D10 (ILL, Grenoble) and D23 (CEA CRG ILL, Grenoble). Both were equipped with a four-circle cryostat, and a wavelength of 2.36 Å was selected from a pyrolytic graphite monochromator.

Symmetry analysis
The magnetic structure models, in particular the coupling of Fourier coefficients between magnetic moments in the unit cell, as well as the derivation of the order parameters in the different symmetry-allowed magnetic domains were carried out using symmetry/representation analysis. Illustrative and pedagogic examples for analog considerations on other compounds are presented in (*35*).

Theory
Theoretical analysis of the possible magnetic states compatible with the propagation vector $\mathbf{q} = (q_x\ 0\ q_z)$ and phase transitions between them was performed on the basis of Landau theory by minimization of the thermodynamic potential built as its invariant (with respect to the paramagnetic group) expansion for the order parameters up to eighth order. As a result, various phase diagrams in the parameter space of temperature-dependent coefficients for quadratic terms of the order parameters in the potential were obtained.

SUPPLEMENTARY MATERIALS
Supplementary material for this article is available at http://advances.sciencemag.org/cgi/content/full/6/7/eaay7661/DC1

Section S1. Symmetry analysis in the extended little group (paramagnetic symmetry)
Section S2. Order parameters in magnetic domains
Section S3. Confirmation of the AF1 and AF2 phases
Section S4. Incompatibility of the AF3 phase with a single irreducible representation
Section S5. Theoretical explanation of the proposed AF3 phase
Fig. S1. Order parameter in magnetic domains.
Fig. S2. Temperature dependence of magnetic Bragg intensities.
Fig. S3. Theoretical phase diagrams.
Table S1. Transformation properties of the complex order parameters S_1 and S_2 in the extended little group (paramagnetic group).
Table S2. Basis vectors S_{nx} of the irreducible representations Γ_n.
Table S3. Observed and calculated polarization matrix elements in the AF1, AF2, and AF3 phases.

REFERENCES AND NOTES
1. S.-W. Cheong, M. Mostovoy, Multiferroics: A magnetic twist for ferroelectricity. *Nat. Mater.* **6**, 13–20 (2007).
2. N. A. Spaldin, R. Ramesh, Advances in magnetoelectric multiferroics. *Nat. Mater.* **18**, 203–212 (2019).
3. T. Kimura, Y. Sekio, H. Nakamura, T. Siegrist, A. P. Ramirez, Cupric oxide as an induced-multiferroic with high-T_c. *Nat. Mater.* **7**, 291–294 (2008).
4. B. Kundys, A. Maignan, C. Simon, Multiferroicity with high-T_C in ceramics of the YBaCuFeO$_5$ ordered perovskite. *Appl. Phys. Lett.* **94**, 072506 (2009).
5. M. Morin, E. Canévet, A. Raynaud, M. Bartkowiak, D. Sheptyakov, V. Ban, M. Kenzelmann, E. Pomjakushina, K. Conder, M. Medarde, Tuning magnetic spirals beyond room temperature with chemical disorder. *Nat. Commun.* **7**, 13758 (2016).
6. T. Shang, E. Canévet, M. Morin, D. Sheptyakov, M. T. Fernández-Díaz, E. Pomjakushina, M. Medarde, Design of magnetic spirals in layered perovskites: Extending the stability range far beyond room temperature. *Sci. Adv.* **4**, eaau6386 (2018).
7. J. B. Forsyth, P. J. Brown, M. B. Wanklyn, Magnetism in cupric oxide. *J. Phys. C: Solid State Phys.* **21**, 2917–2929 (1988).
8. B. X. Yang, T. R. Thurston, J. M. Tranquada, G. Shirane, Magnetic neutron scattering study of single-crystal cupric oxide. *Phys. Rev. B* **39**, 4343–4349 (1989).
9. P. J. Brown, T. Chattopadhyay, J. B. Forsyth, V. Nunez, Antiferromagnetism in CuO studies by neutron polarimetry. *J. Phys. Condens. Matter* **3**, 4281–4287 (1991).
10. M. Ain, A. Menelle, B. M. Wanklyn, E. F. Bertaut, Magnetic-structure of CuO by neutron-diffraction with polarization analysis. *J. Phys. Condens. Matter* **4**, 5327–5337 (1992).
11. Z. Wang, N. Qureshi, S. Yasin, A. Mukhin, E. Ressouche, S. Zherlitsyn, Y. Skourski, J. Geshev, V. Ivanov, M. Gospodinov, V. Skumryev, Magnetoelectric effect and phase transitions in CuO in external magnetic fields. *Nat. Commun.* **7**, 10295 (2016).
12. H. Katsura, N. Nagaosa, A. V. Balatsky, Spin current and magnetoelectric effect in noncollinear magnets. *Phys. Rev. Lett.* **95**, 057205 (2005).
13. I. A. Sergienko, E. Dagotto, Role of the Dzyaloshinskii-Moriya interaction in multiferroic perovskites. *Phys. Rev. B* **73**, 094434 (2006).
14. M. Mostovoy, Ferroelectricity in spiral magnets. *Phys. Rev. Lett.* **96**, 067601 (2006).
15. R. Villarreal, G. Quirion, M. L. Plumer, M. Poirier, T. Usui, T. Kimura, Magnetic phase diagram of CuO via high-resolution ultrasonic velocity measurements. *Phys. Rev. Lett.* **109**, 167206 (2012).
16. G. Giovannetti, S. Kumar, A. Stroppa, J. van den Brink, S. Picozzi, J. Lorenzana, High-T_c ferroelectricity emerging from magnetic degeneracy in cupric oxide. *Phys. Rev. Lett.* **106**, 026401 (2011).
17. G. Jin, K. Cao, G.-C. Guo, L. He, Origin of ferroelectricity in high-T_c magnetic ferroelectric CuO. *Phys. Rev. Lett.* **108**, 187205 (2012).
18. P. Tolédano, N. Leo, D. D. Khalyavin, L. C. Chapon, T. Hoffmann, D. Meier, M. Fiebig, Theory of high-temperature multiferroicity in cupric oxide. *Phys. Rev. Lett.* **106**, 257601 (2011).
19. I. N. Apostolova, A. T. Apostolov, S. G. Bahoosh, J. M. Wesselinova, S. Trimper, Multiferroicity in the dielectric function of CuO. *Phys. Status Solidi Rapid Res. Lett.* **7**, 1001–1004 (2013).
20. P. Babkevich, A. Poole, R. D. Johnson, B. Roessli, D. Prabhakaran, A. T. Boothroyd, Electric field control of chiral magnetic domains in the high-temperature multiferroic CuO. *Phys. Rev. B* **85**, 134428 (2012).

21. H. Jacobsen, S. M. Gaw, A. J. Princep, E. Hamilton, S. Tóth, R. A. Ewings, M. Enderle, E. M. H. Wheeler, D. Prabhakaran, A. T. Boothroyd, Spin dynamics and exchange interactions in CuO measured by neutron scattering. *Phys. Rev. B* **97**, 144401 (2018).

22. G. Lawes, M. Kenzelmann, N. Rogado, K. H. Kim, G. A. Jorge, R. J. Cava, A. Aharony, O. Entin-Wohlman, A. B. Harris, T. Yildirim, Q. Z. Huang, S. Park, C. Broholm, A. P. Ramirez, Competing magnetic phases on kagomé staircase. *Phys. Rev. Lett.* **93**, 247201 (2004).

23. G. Lawes, A. B. Harris, T. Kimura, N. Rogado, R. J. Cava, A. Aharony, O. Entin-Wohlman, T. Yildirim, M. Kenzelmann, C. Broholm, A. P. Ramirez, Magnetically driven ferroelectric order in Ni$_3$V$_2$O$_8$. *Phys. Rev. Lett.* **95**, 087205 (2005).

24. O. Heyer, N. Hollmann, I. Klassen, S. Jodlauk, L. Bohatý, P. Becker, J. A. Mydosh, T. Lorenz, D. Khomskii, A new multiferroic material: MnWO$_4$. *J. Phys.: Condens. Matter* **18**, L471–L475 (2006).

25. I. Urcelay-Olabarria, J. M. Perez-Mato, J. L. Ribeiro, J. L. García-Muñoz, E. Ressouche, V. Skumryev, A. A. Mukhin, Incommensurate magnetic structures of multiferroic MnWO$_4$ studied within the superspace formalism. *Phys. Rev. B* **87**, 014419 (2013).

26. M. Kenzelmann, A. B. Harris, A. Aharony, O. Entin-Wohlman, T. Yildirim, Q. Huang, S. Park, G. Lawes, C. Broholm, N. Rogado, R. J. Cava, K. H. Kim, G. Jorge, A. P. Ramirez, Field dependence of magnetic ordering in Kagomé-staircase compound Ni$_3$V$_2$O$_8$. *Phys. Rev. B* **74**, 014429 (2006).

27. V. P. Sakhnenko, N. V. Ter-Oganessian, Praphase concept for the phenomenological description of magnetoelectrics. *Crystallogr. Rep.* **57**, 112–117 (2012).

28. A. Rebello, Z. C. M. Winter, S. Viall, J. J. Neumeier, Multiple phase transitions in CuO observed with thermal expansion. *Phys. Rev. B* **88**, 094420 (2013).

29. P. J. Brown, Spherical neutron polarimetry, in *Neutron Scattering from Magnetic Materials*, T. Chatterji, Ed. (Elsevier, 2005), chap. 5, pp. 215.

30. T. Hoffmann, K. Kimura, T. Kimura, M. Fiebig, Second harmonic generation spectroscopy and domain imaging of the high-temperature multiferroic CuO. *J. Physical Soc. Japan* **81**, 124714 (2012).

31. N. Qureshi, *Mag2Pol*: A program for the analysis of spherical neutron polarimetry, flipping ratio and integrated intensity data. *J. Appl. Cryst.* **52**, 175–185 (2019).

32. V. S. Maryasin, M. E. Zhitomirsky, Order from structural disorder in the *XY* pyrochlore antiferromagnet Er$_2$Ti$_2$O$_7$. *Phys. Rev. B* **90**, 094412 (2014).

33. A. Andreanov, P. A. McClarty, Order induced by dilution in pyrochlore XY antiferromagnets. *Phys. Rev. B* **91**, 064401 (2015).

34. J. Gaudet, A. M. Hallas, D. D. Maharaj, C. R. C. Buhariwalla, E. Kermarrec, N. P. Butch, T. J. S. Munsie, H. A. Dabkowska, G. M. Luke, B. D. Gaulin, Magnetic dilution and domain selection in the *XY* pyrochlore antiferromagnet Er$_2$Ti$_2$O$_7$. *Phys. Rev. B* **94**, 060407(R) (2016).

35. L. C. Chapon, An introduction to the use of representation analysis for studying magnetoelectrics and multiferroics. *EPJ Web Conf.* **22**, 00013 (2012).